Estuaries and Coasts
https://doi.org/10.1007/s12237-020-00828-8

SPECIAL ISSUE: SHALLOW WATER MAPPING

Quantifying Vegetation and Landscape Metrics with Hyperspatial Unmanned Aircraft System Imagery in a Coastal Oligohaline Marsh

Whitney P. Broussard III[1,2] · Jenneke M. Visser[1,3] · Robert P. Brooks[4]

Received: 13 July 2019 / Revised: 26 August 2020 / Accepted: 3 September 2020

Abstract
Billions of dollars are projected to be spent on restoration projects along the northern Gulf Coast which will require efficient monitoring at both landscape and project-specific scales. Recent developments in unmanned aircraft systems (UAS) have sparked interest in the ability of these "drones" to capture hyperspatial imagery (pixel resolution < 10 cm) that resolves individual species and produces accurate data for monitoring programs in coastal landscapes. We present a case study conducted at Coastwide Reference Monitoring System (CRMS) station 0392, a *Spartina patens*–dominated, oligohaline coastal marsh in Terrebonne Parish, Louisiana. Results demonstrate the ability of UAS technology to collect hyperspatial, multispectral aerial images in a coastal wetland, and to produce very-high-resolution orthomosaics and digital elevation models. We then used object-based image analysis (OBIA) techniques to (1) delineate the land–water interface, (2) classify composition by dominant species, and (3) quantify average plant height by species. Model results were validated with traditional on-the-ground CRMS vegetation surveys. Results suggest that OBIA methods can overcome the spectral variability of hyperspatial datasets, quantify uncertainties in conventional techniques, and provide improved estimates of wetland vegetation cover and species composition. These methods scale conventional plot-level coverage values to data-rich landscape-level models and provide useful tools to monitor restoration performance, landscape changes, and ecosystem services in coastal wetland systems.

Keywords Unmanned aircraft systems · Object-based image analysis · Coastal wetlands · Vegetation mapping · Land–water interface · Landscape patterns · Ecosystem services

Introduction

Coastal wetlands are important for many reasons. They are naturally occurring and hold intrinsic value (Golley 1987) while offering valuable ecosystem services to communities near and far (Costanza et al. 1997; Brooks et al. 2007). Louisiana's coastal wetlands account for roughly 22% of the total coastal wetland area of the lower 48 conterminous United States (Gosselink 1984). They provide habitat for 5 million migratory waterfowl annually, support 26% of the continental US commercial fisheries landings by weight, and protect one of the most productive oil and gas regions in the country (CPRA 2012). The wetland loss crisis in coastal Louisiana claimed 4833 km^2 (1866 mi^2) of land from 1932 to 2016 (Couvillion et al. 2017) and has the potential to lose up to an additional 4532 km^2 (1750 mi^2) of land in the next 50 years (CPRA 2012). The causes of land loss in Louisiana are complex and driven by both natural and human factors. Relative sea-level rise as a result of global rise in sea level (Church and White 2006) and local subsidence (Meckel et al. 2006) have been identified as the main drivers (González and Tornqvist 2006).

Wetlands have the capacity to keep up with relative sea-level rise, i.e., when positive vertical accretion is equivalent to or greater than sea-level and subsidence changes, provided

Communicated by Richard C. Zimmerman

Electronic supplementary material The online version of this article (https://doi.org/10.1007/s12237-020-00828-8) contains supplementary material, which is available to authorized users.

✉ Whitney P. Broussard, III
wbroussard@jescous.com

1 Institute for Coastal and Water Research, University of Louisiana at Lafayette, Lafayette, LA, USA

2 Present address: JESCO, Inc., Jennings, LA, USA

3 School of Geosciences, University of Louisiana at Lafayette, Lafayette, LA, USA

4 Riparia, Department of Geography, Pennsylvania State University, University Park, PA, USA

that the plants produce organic input for soil formation and assist with the trapping of inorganic sediment (Morris et al. 2002; Wang et al. 2019). Species composition combined with vegetation cover and biomass are important, quantifiable determinants that can be monitored through time to determine the ability of a marsh to maintain itself (Chamberlain and Ingram 2012; Cretini et al. 2012; Schoolmaster et al. 2018).

Monitoring of species composition at the landscape level has historically relied upon field observations such as ocular estimates of dominant species identification and coverage (i.e., Braun–Blanquet cover scale (Kent and Coker 1994)). This is a laborious process based on the determinations of vegetation experts (Acosta et al. 2005; Sasser et al. 2014). Such surveys are costly and infrequent, often every 5 to 10 years. Remote sensing workflows have many benefits over traditional field surveys including increased temporal resolution and automation of the species identification process using big data and machine learning techniques.

The Ramsar Convention on Wetlands supports the development and application of remote sensing and GIS to fill gaps in baseline wetland inventories (Rebelo et al. 2009). Multispectral and hyperspectral image analyses have mapped coastal wetland vegetation, submerged aquatic vegetation, and coral reefs (Phinn et al. 1996; Belluco et al. 2006; Chust et al. 2008; Yang and Artigas 2010), and identified invasive vegetation in a wetland deltaic ecosystem (Hestir et al. 2008). Multi-temporal satellite imagery, combined with field-verified spectral and Lidar data, have been used to map marsh vegetation (Gilmore et al. 2008; Mitchell et al. 2014). Couvillion et al. (2017) used a combination of aerial and satellite data to map coastal land loss from 1932 to 2016. Recent advancements in object-based image analysis are being used to extract coastlines from high-resolution satellite data (Giannini and Parente 2015). European Remote Sensing satellite radar data has been used to estimate wetland vegetation biomass (Moreau and Le Toan 2003). Traditional remote sensing techniques have been used to map landscape fragmentation and the land–water interface in Louisiana's coastal zone (Suir et al. 2013; Couvillion et al. 2017), develop coastal vegetation maps by species, and map marsh health using indicators such as the Normalized Difference Vegetation Index (NDVI) (Steyer et al. 2013).

Unmanned aircraft system (UAS, also known as unmanned aerial system or unmanned aerial vehicle) technology has witnessed rapid growth in monitoring of coastal environments (Klemas 2015) due, in part, to advancements in commercial "off-the-shelf" hardware, software, GPS navigation, command and control, sensors, and optics (Pereira et al. 2009). In the late 1970s, Przybilla and Wester-Ebbinghaus (1979) completed the first photogrammetry experiments using a fixed-wing remotely controlled aircraft. Eisenbeiss (2004) was the first to create a high-resolution digital terrain model using a commercial low-cost model helicopter with semi-automated navigation. In coastal environments, high-precision elevation models derived from UAS datasets are improving physical and geomorphological studies. For example, Chong (2007) mapped local beach erosion, Lejot et al. (2007) mapped channel bathymetry and topography, and Niethammer et al. (2012) mapped changes in topography after a landslide. Lidar data and photogrammetrically derived elevation models are also improving classification processes and image analysis by adding high-resolution digital surface models and digital elevation models to conventional image data stacks (Chust et al. 2008; Yang and Artigas 2010; Yang and Chen 2015; Sankey et al. 2017).

Remote sensing analytics can be applied to UAS datasets and improve habitat mapping, landscape pattern analysis, and coastal vegetation studies. Multispectral and hyperspectral UAS imagery are now regularly used to image, classify, and map wetlands (Lechner et al. 2012; Klemas 2015; Ahmed et al. 2017). Object-based techniques are used to map mangrove habitat (Cao et al. 2018), wetland vegetation (Pande-Chhetri et al. 2017; Husson et al. 2016), and upland swamps (Lechner et al. 2012) among others. High-resolution UAS datasets also improve estimates of vegetation parameters like biomass (Doughty and Cavanaugh 2019).

Comparing traditional ground surveys, aerial photogrammetry, and satellite data analysis is complex. Each data source and subsequent workflow has a niche within the broader scientific community and can offer a suitable methodology for various projects. There are tradeoffs to consider such as cost, area covered, resolution, and the potential for high temporal sampling (Broussard et al. 2018). Manned aircraft overflights, for example, can be costly (Klemas 2013) as compared with UAS technology on smaller areas of interest. However, manned aircraft can cover and map larger areas of interest at a lesser cost per hectare because of economies of scale. UAS have the capacity to improve the spatial resolution of imagery (1–10 cm) with the added bonus of flexible deployments that improve the temporal resolution of these datasets (Lechner et al. 2012; Niethammer et al. 2012; Klemas 2015; Marcaccio et al. 2015).

For monitoring coastal wetlands along the Northern Gulf Coast, there are several sources of remotely captured data at various spatial scales that can fill in the data gaps between coastwide helicopter surveys (Sasser et al. 2014) and site-specific surveys like the Coastwide Reference Monitoring System (CRMS) network (Steyer 2010). These data types include LANDSAT satellite imagery (30 m), Worldview satellite imagery (40–50 cm), traditional aerial photography (30 cm–1 m), and UAS-captured aerial photography (2–10 cm). Figure 1 demonstrates a typical aerial image basemap with 1-m resolution compared to 2.5-cm resolution UAS imagery collected at the same location. Such hyperspatial, or

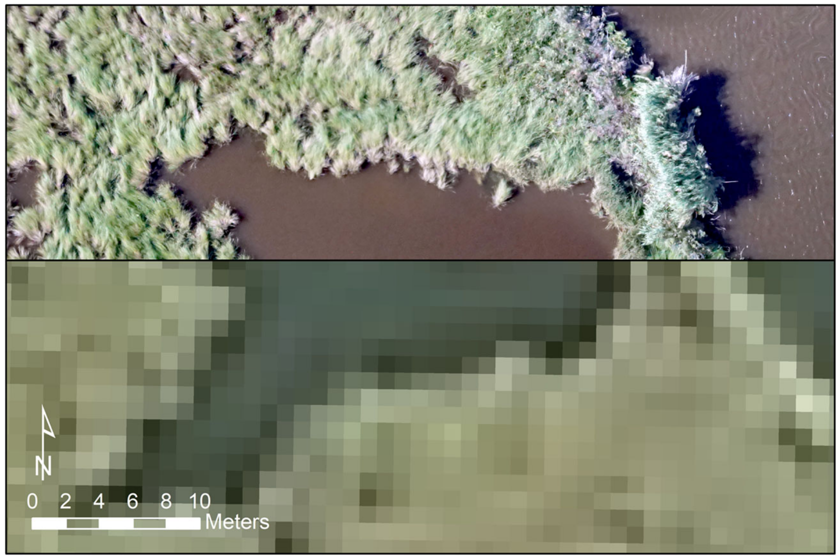

Fig. 1 2.5-cm resolution UAS imagery collected in 2106 (above) and 1-m resolution aerial photography (below) collected as part of the Coastal Wetlands Planning, Protection and Restoration Act program (CWPPRA 2008) shown here as a "slider window" of the same scene. Note the *Spartina patens*–dominated marsh and the tall *Phragmites australis* along the water's edge

very-high-resolution, datasets allow a user to discern patterns and objects with detail similar to on-the-ground surveys. The question here is whether such data products can be used in an automated workflow to reliably classify and map intricate observations of wetland vegetation over larger, regional areas. If so, then documenting fluctuations in landscape patterns and the cover and height of specific plant communities would not only enhance wetland inventories but link these observations to differential levels of ecosystem services provided by these communities. Such services include carbon sequestration (Nahlik and Fennessy 2016; Wang et al. 2019), retention of sediments in support of marsh accretion (Morris et al. 2016), effectiveness of vegetation in attenuating storm surge (Chatagnier 2012), changes in biodiversity support (e.g., plant species richness) (Cretini et al. 2012), and shifting habitat suitability for breeding and wintering bird species (DeLuca et al. 2008; Woodrey et al. 2012; Valdes et al. 2016).

Research Objective

The objective of the present study was to investigate the feasibility of collecting UAS data in a coastal Louisiana grass-dominated marsh and to determine the usability of hyperspatial, multispectral imagery for vegetation mapping. Such improvements would be important steps toward a comprehensive monitoring program of coastal zones. Specifically, the team addressed the following research question: *Can UAS hyperspatial imagery be used to classify species composition, model the land–water interface, and quantify certain productivity estimates, particularly plant height, in a Spartina patens–dominated oligohaline coastal marsh environment?*

Methods

A pilot project was conducted in Terrebonne Parish, Louisiana, with the following general workflow: (1) collect 2.5 cm resolution UAS imagery using red–green–blue and near-infrared sensors of a 1-km^2 area in a coastal marsh; (2) create georeferenced orthomosaic and digital surface model (DSM) raster datasets; (3) use object-based image analysis to model the land–water interface, dominant species distribution, and plant height; (4) quantify the model accuracy using ground-based vegetation survey measurements (species cover, composition, and height) and conventional spatial techniques (land–water interface).

Study Area

The project site was a degraded oligohaline wiregrass marsh (Visser et al. 1998) located in Terrebonne Parish, Louisiana, along the Northern Gulf of Mexico, north of Lake Boudreaux, and east of Bayou Grand Calliou (Fig. 2). The site is part of the Terrebonne Bay drainage basin in the Mississippi River Deltaic Plain. The area is prone to high rates of subsidence and land loss (Couvillion et al. 2017). A benefit of the present study area is that there is one long-term monitoring site belonging to the CRMS program (Steyer 2010) within the project boundary. This station, 0392, was used as a reference dataset since it has on-the-ground sampling stations for species cover and regularly calculated land–water areas based on traditional aerial photography. The 1-km^2 area around CRMS site 0392 was the area of the data acquisition for the present study (CPRA 2016, Fig. 2). This site is one of the most fragmented and variable sites in the CRMS network and a good candidate for testing the ability of UAS workflows to map and model a highly fragmented and dynamic landscape.

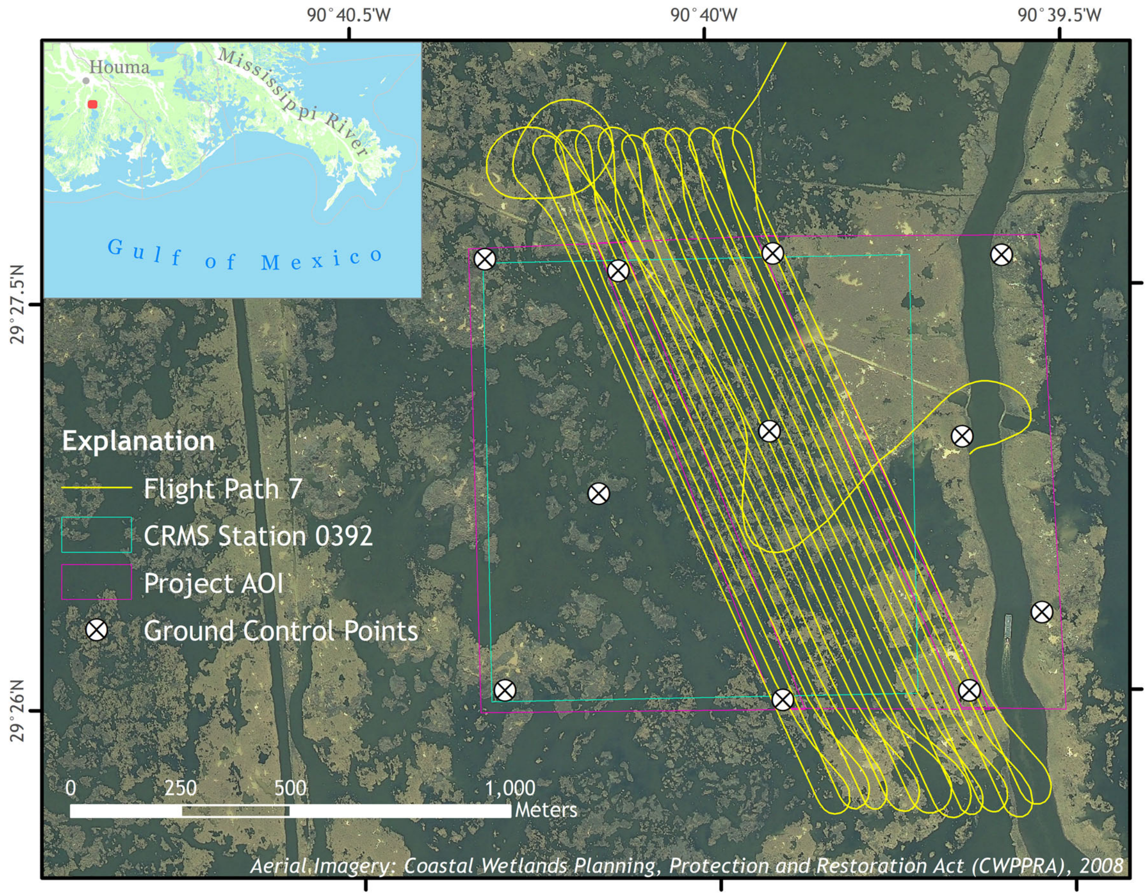

Fig. 2 Location map of the project site including one set of flight lines in yellow, ground control points in white/black, and the 1-km^2 area of interest (AOI) surrounding CRMS 0392 in cyan. The landing location is 4 km north of the AOI in an open upland field

Fieldwork was completed August 29 and 30, 2016, and fully compliant with the Federal Aviation Administration (FAA) Small Unmanned Aircraft Rule (Part 107), which coincidentally was effective August 29, 2016. The area of interest (AOI) was divided into three flight blocks. Each block required approximately 35 min to complete, which allowed 15 min of additional flight time for emergency maneuvers and travel to the landing location. Ground control point (GCP) aerial targets were distributed evenly throughout all three flight blocks (Fig. 2). So as not to disturb the target vegetation, 60 × 60 cm vinyl sheets with an iron cross pattern were fixed atop wooden stakes and elevated with a fixed center for supporting GPS equipment (Fig. 3). The center point was then surveyed using high-precision GPS equipment with real-time kinematic corrections delivered via a virtual reference station network (GPS horizontal accuracy = 3 cm, vertical accuracy = 6 cm).

Data Collection

UAS imagery was acquired with a Trimble UX5 aerial imaging rover (Fig. 4) carrying two commercial-grade, off-the-shelf cameras and controlled using a Trimble Yuma tablet with Trimble Aerial Imaging software. Specifically, we used a Sony α5100 camera that combines red, green, and blue sensors (350–750 nm) to create true color (RGB) image pixels. A modified Sony NEX-5r camera was used to capture near-infrared (760–820 nm), red (630–690 nm), and green (520–580 nm) light to create color infrared (CIR) image pixels. This setup required separate flights for each camera.

Fig. 3 Ground control point positioned above the target vegetation

Fig. 4 Trimble UX5 aerial imaging rover used in this project

The Sony NEX-5r was modified by replacing the internal hot mirror filter with a filter that allows transmittance of near-infrared light, coupled with a blue rejection filter on the lens. The modification allows red and green sensors to pick up small amounts of near-infrared reflectance (700–1100 nm), but forces the blue-specific sensors to record near-infrared reflectance only. Both cameras used a Voigtländer lens with a fixed nominal focal length of 15 mm. A flying altitude of 75 m resulted in a raw ground sample distance (resolution) of 2.33 cm for the CIR sensor and 1.95 cm for the RGB sensor. The catapult launcher was secured to the bow of a research vessel, and the UX5 was launched over the water within the AOI. Because the study area was a highly degraded marsh, there was no logical landing location near the AOI. An appropriate location for a belly landing was identified 4 km north (Fig. 2). To maintain radio communications and line of sight between the aerial rover and the ground control station, the project team chased the rover home to the landing location using an airboat. Four flights were flown over 2 days with a side lap of 80% and a forward lap of 85%. The results presented here represent two of those flights, both of which are from the same flight block. One contains the RGB dataset, and the other contains the CIR dataset.

Post-Processing

Trimble-Inpho UAS Master Software (Trimble Inc 2016a) was the photogrammetric software used to process the UAS imagery and generate orthomosaic and DSM raster datasets. Over 1000 images were collected per flight. Each raw image was tagged with an initial orientation defined by the latitude, longitude, and altitude measured by the internal GPS unit and the roll, pitch, and yaw of the aircraft as measured by the airframe's inertial measurement unit. These initial approximations of the image's orientation were then used by the photogrammetry software to calibrate the camera focal length, principal point, and distortion parameters. The images were then aligned, and tie point locations were extracted, i.e., those discernible locations that can be identified in multiple photos, using Structure-from-Motion algorithms (Westoby et al. 2012; Mancini et al. 2013). Each GCP was then located and manually selected within each available picture to refine the initial orientation and to tightly georeference the orthomosaics to a datum. After the absolute orientation process was completed, the root mean square error compared with the horizontal and vertical control was 2.40 and 2.42 cm, respectively, and the 95% confidence level for the horizontal and vertical control was 4.83 and 4.74 cm, respectively. Final RGB, CIR, and DSM datasets are presented in Fig. 5. The ground sample distance of both orthomosaics was 2.5 cm while the DSM generated a ground sample distance of 7.2 cm. For more information on quality control and error estimation of UAS data, see the ASPRS Positional Accuracy Standards for Digital Geospatial Data (ASPRS 2015) and Abdullah et al. (2015).

Object-Based Image Analysis

Object-based image analysis (OBIA) classification methods are a good fit for UAS imagery (e.g., Laliberte and Rango 2009). Initially developed for coarser datasets, the ability of OBIA to scale to finer UAS imagery is encouraging. With high-resolution datasets, spectral variance increases within target classes (Marceau and Hay 1999; Blaschke 2010). Spectral separation between the classes is, therefore, more difficult to identify and classify. Similar to the way in which humans interpret an image, OBIA methods address spectral variability and scaling issues by segmenting or grouping finer pixels into larger, recognizable image objects that maximize homogeneity and minimize heterogeneity. The pixels within an object share similar attributes such as spectral signature, texture, shape, and context to other objects (Blaschke 2010; O'Neil-Dunne et al. 2014). This technique makes the classification of UAS imagery easier because the programmer is then tasked with finding commonalities by object (hundreds to thousands of grouped pixels per object) rather than by individual pixel (in this case 2.5 cm on the ground or 1.6 billion pixels per 1 km^2).

The goal of the OBIA in the present study was the delineation of marsh grass versus open water, the identification of dominant vegetation species, and the calculation of plant height by dominant species using hyperspatial, multispectral UAS imagery. The analysis first classified objects as either land or water and then further separated those land objects into one of three vegetation categories: (1) SPPA, *Spartina patens*; (2) PHAU7, *Phragmites australis*; (3) OTHER, a mix of *Bacopa monnieri*, *Pluchea odorata*, *Iva frutescens*, and *Baccharis halimifolia*. Figure 6 demonstrates the outlines of objects identified in the UAS imagery. The objects were

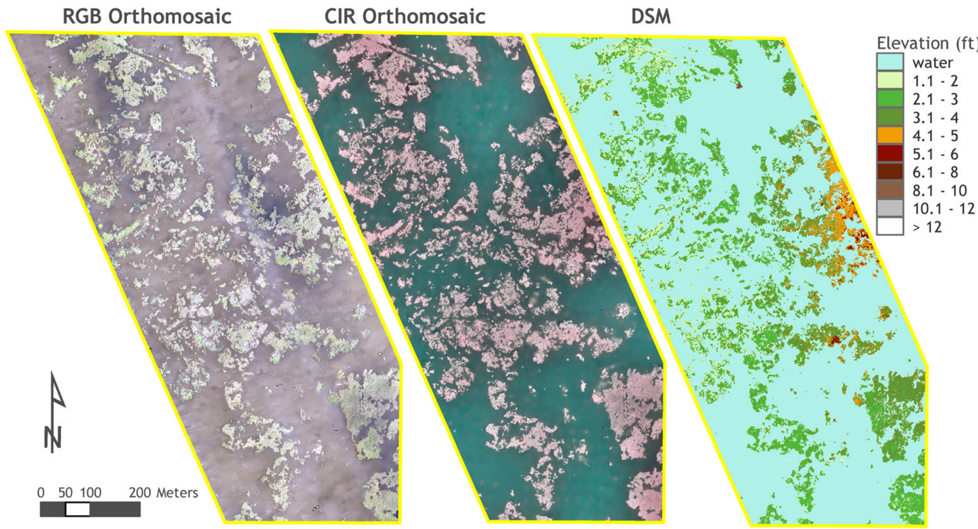

Fig. 5 Red–green–blue (left) and color infrared (center) and DSM raster datasets generated from UAS imagery over the project site

delineated using Trimble eCognition Developer software (Trimble Inc 2016b) based on similar spectral and texture values, average height of the cells within objects, as well as the context of other neighboring objects. Unique characteristics of objects within each target class were then identified through interpretation and exploration of the imagery. Based on these characteristics, a rule set of hierarchical algorithms (see Online Resource 1) was developed to methodically classify objects into one of the three target classes.

The intensity of the near-infrared spectrum coupled with the very small pixel size of the UAS imagery made the identification of the water objects straightforward. Because water absorbs near-infrared wavelengths, we used a simple threshold of CIR intensity and classified those objects with a mean near-infrared reflectance value lower than the threshold as water. For the identification and classification of dominant vegetation species, the algorithms focused first on plant height, then greenness, and finally texture. Because *Phragmites australis*, the common reed, is a tall clumping species, this PHAU7 class was initially identified by plant height (i.e., objects that were taller than their surrounding objects). The class OTHER was initially identified by a greenness factor because this class of plants was visibly greener than the surrounding grasses. Finally, after classifying both the PHAU7 and OTHER classes, the remaining objects belonging to the larger land class were then classified as SPPA.

An accuracy assessment was performed using two methods. The first was a stratified random sampling in which a predetermined number of random coordinate points were generated within each group based on the relative aerial extent

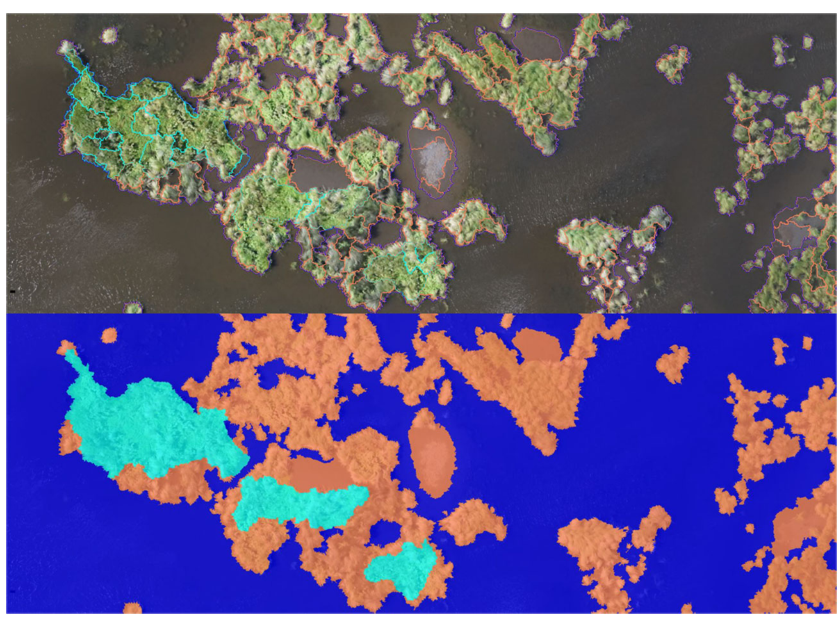

Fig. 6 Objects outlined (above) and then classified (below) demonstrate the ability of hyperspatial datasets to capture a complex land–water interface and species diversity. Blue is the class WATER, teal is the class OTHER, and orange is the class SPPA

of each group (50 Water, 50 SPPA, 20 OTHER, and 10 PHAU7). We then performed a manual photo interpretation based on the UAS orthomosaics to determine if the model properly classified the image at each pre-determined location. The second method verifies the models generated by the present study with publicly available datasets obtained from CRMS site 0932. Specifically, the researchers compared the predicted land–water ratio derived from UAS data and the predicted land–water ratio published by the CRMS program. The CRMS land–water product utilizes a pixel-based approach and traditional aerial photography with roughly 1-m ground sample distance. The products presented here were developed using an object-based image analysis using UAS aerial photography with roughly 2.5 cm ground sample distance. In addition to a comparison of remote sensing products, predicted vegetation class and vegetation height derived from UAS datasets were compared with observed on-the-ground vegetation species composition and field measured plant height. All CRMS data were collected in the late summer of 2016 during peak biomass (9/1/16 for vegetation), similar to the timing of the UAS data collections. CRMS output is delivered through the Coastal Information Management System database and is publicly available (CPRA 2016).

The publicly available CRMS data are based on vegetation samples collected at three sites along a transect within the CRMS 0932 boundary (Fig. 7). The subsample sites are 4-m^2 quadrants whose locations were measured using a handheld GPS in the field with roughly 3-m accuracy. CRMS personnel measure the average height of the vegetation in the field as the length of the stems to the nearest centimeter. Ten subsample sites were established when the CRMS program began in 2006, but due to rapid land loss at this site, only three were vegetated when the present study was performed. The remaining seven were open water.

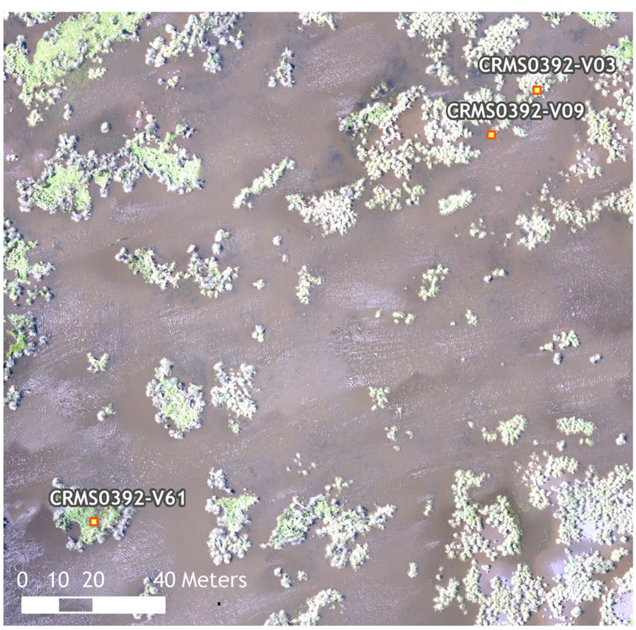

Fig. 7 Three subsample sites (V03, V09, and V61) in the project area demonstrate the fragmented herbaceous marsh landscape

Plant height was estimated as the difference between the modeled DSM (i.e., average elevation of the top of the plants) and the elevation of the marsh surface. To estimate the marsh surface, we used the average ground elevation measured by the CRMS program for the site (mean elevation = 6.98 cm (0.229 ft) above Geoid12A).

Results

Image Classification Assessment

Results from the image classification assessment are presented as an error matrix in Table 1. Overall accuracy was 85%, and the Kappa coefficient was 0.78. User's Accuracy ranged from 67% for OTHER to 100% for PHAU7. Producer's Accuracy ranged from 73% for SPPA to 100% for Water. This Producer's Accuracy for Water is noteworthy because it means that the simple approach to classifying water, i.e., a single threshold of near-infrared reflectance, is satisfactory. The fine-scaled, 2–6 cm, delineation between the land–water interface is a significant improvement in coastal land loss mapping efforts. Each 2–6 cm pixel is either land or water. There is very little mixing of spectral signatures within UAS orthophoto pixels as compared with the mixing found in traditional 1-m aerial photographs (Fig. 1). As such, the land–water interface model is highly accurate and reliable.

CRMS Land–Water Analysis

The land–water classification models produced by CRMS and in the present study were compared (Fig. 8, Table 2). The estimates of percent land were reasonably close between the CRMS model and the project study model, which was unexpected given the substantial difference in resolution between the two datasets and the difficulties in delineating the land–water interface when 1-m pixels along the marsh edge are a mix of land and water spectral signatures. The main difference was that the coarser aerial photography datasets are not able to resolve small interior ponds (Enwright et al. 2014) and tended to overestimate land. Table 2 demonstrates the overestimation of land in the CRMS model and the ability of the high-fidelity UAS dataset to capture the complex land–water interface and resolve the smaller pockets of open water in the interior marsh.

CRMS Vegetation Classification

Vegetation communities were compared between the predicted UAS vegetation class model and the observed CRMS data at each of three subsample sites (V03, V09, and V61) located

Table 1 Error matrix demonstrating the results from the accuracy assessment of the object-based image analysis

Reference class							
Predicted class		WATER	SPPA	OTHER	PHAU7	Count	Producer's Accuracy (%)
	WATER	**49**	0	0	0	49	100
	SPPA	7	**35**	6	0	48	73
	OTHER	2	2	**16**	0	20	80
	PHAU	0	0	2	**8**	10	80
	Count	58	37	24	8	127	
	User's Accuracy (%)	84	95	67	100		
	Overall accuracy: 85% Kappa coefficient: 0.78						

Bold values indicate the number of samples within a class where the predicted model matched the reference dataset

within the CRMS 0392 boundary (CPRA 2016). The predicted vegetation model was queried at each location and compared with the cover reported in the CRMS dataset. Species observed during the CRMS ground survey are listed in order of their cover. The comparisons are as follows: V03—predicted SPPA, measured *Spartina patens*, *Amaranthus australis*, and *Cyperus odoratus*; V09—predicted SPPA, measured *Spartina patens*; V61—predicted OTHER, measured *Bacopa monnieri*, *Eleocharis parvula*, and *Pluchea odorata*. Largely a demonstration exercise because of the low sample size, the predicted dominant vegetation did match the observed dominant vegetation on the ground at each sampled location.

Plant Height

Plant heights measured in the field and modeled based on UAS data are as follows: V03—predicted 1.30 m, measured 1.48 m; V09—predicted 0.43 m, measured 1.19 m; V61—predicted 0.46 m, measured 0.49 m. Vertical error associated with field measurements are ± 10 cm due to averaging of surrounding plant stem height by field personnel. Vertical error associated with predicted heights are ± 8 cm due to errors associated with photogrammetrically derived elevation estimates of modeled objects and error associated with GPS equipment used for control. Based on this comparison, there was less than 20 cm difference in plant height between ground measurements and the digital elevation model for two of the three sites. The unsatisfactory site (V09) had a small percentage of land predicted. Because the locations of the subsample sites were determined in the field using rough GPS estimations (± 3 m horizontal), it is highly likely that the modeled dataset was not queried in the exact location as the sites on the ground. A 3-m distance can easily traverse open water, partial plant cover, and complete plant cover in this highly degraded landscape. In addition, the

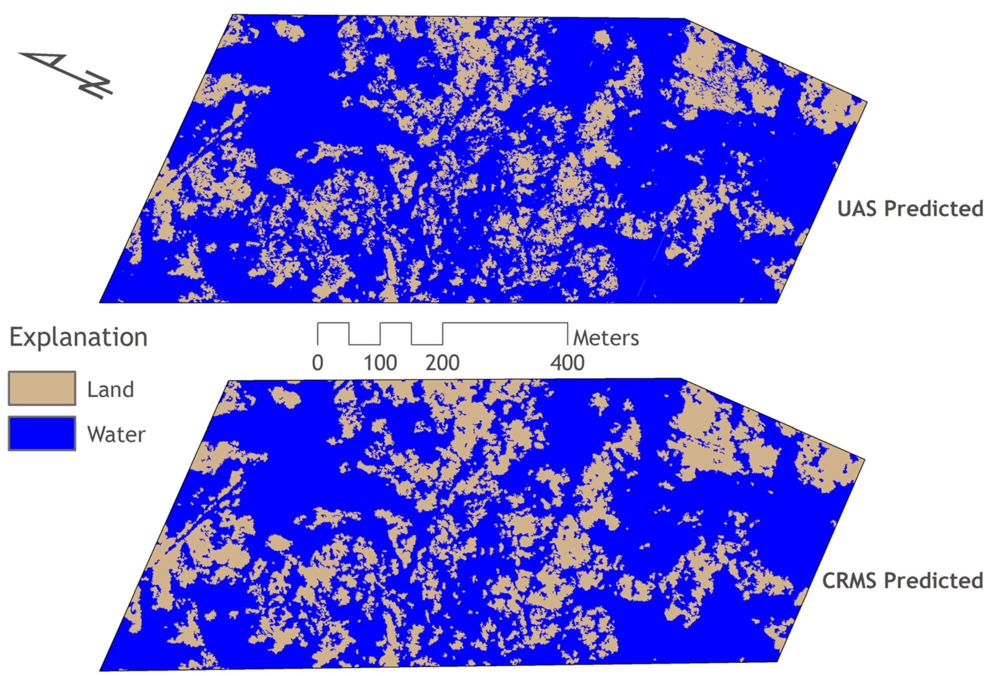

Fig. 8 Land–water classification model produced from 2.5-cm UAS data (top) and traditional 1-m resolution aerial photography that is publicly available through the CRMS program (bottom)

Table 2 Results of the land–water classification comparison between the predicted land–water interface model and the publicly available CRMS land–water analysis dataset

	Land		Water	
	CRMS	UAS	CRMS	UAS
Area (km^2)	0.14	0.12	0.33	0.35
Percent	30%	26%	70%	74%

CRMS ground elevation surveys were performed at 10 random points across the transect and may not reflect the actual elevation at the vegetation subsample sites. In aggregate, however, the methodology shows promise in its ability to estimate plant height at the landscape scale.

Discussion

Hyperspatial datasets allow a user to discern patterns and objects with great detail. Even the shape and size of a broadleaf blade can be observed. Microtopographies with elevation changes on the order of 3–5 cm can be measured in a marsh creation site. There is potential for UAS technology to supplement the coastwide helicopter transects (Sasser et al. 2014) and the Coastwide Reference Monitoring System sites (Steyer 2010) in Louisiana, USA. At present, the 30-day helicopter survey is conducted once every 7 years by a crew of two to four scientists and one or more pilots. Successful implementation of a UAS survey could increase the temporal resolution of the dataset and potentially reduce the cost of deployment. The ability to capture calibrated near-infrared reflectance of the sampling locations could also provide information on the health and vigor of the sampled vegetation using indices such as NDVI, which would be an improvement over current methods. Additional improvements that UAS imagery could provide include the ability to compute a digital elevation model (DEM) of bare earth or marsh elevation based on directly georeferenced UAS-mounted Lidar or photogrammetrically produced point clouds such as those presented here.

Lessons Learned

Operating a UAS in a coastal environment does not come without worry or problems. Potential hurdles include proper locations for takeoff and landing, properly estimating flight times that account for high wind conditions, and communicating with local landowners regarding privacy and permission concerns. Current FAA regulations constrain the UAS to only fly within the line of sight of the pilot in command or designated spotter, and battery limitations constrict the footprint of flight operations and data acquisitions. These current limitations make UAS platforms unsuitable as a coastwide survey technique, but well positioned to supplement site-specific monitoring. If future regulations relax the beyond-line-of-sight requirement, the ability to work from an upland site and capture imagery over coastal wetland sites will be easier and perhaps worthy of long-range, high-endurance UAS investments.

Big data collection, storage, maintenance, and analysis is another consequence of UAS workflows. Data file size increases on a logarithmic scale as ground sample distance increases linearly. Furthermore, the Structure-from-Motion algorithms used in UAS photogrammetric workflows require access to large amounts of computer random access memory (RAM). Manipulating and processing large datasets requires large graphics processing units (GPUs). The time involved with these kinds of workflows often involves overnight computations using modern desktop computers. For these reasons, additional processing time and computational resources are required to convert the raw UAS imagery into accurate points clouds, elevation models, and orthomosaics. Another level of effort is then required to analyze these intermediate deliverables and to develop actionable information.

These limitations notwithstanding, there are several benefits to be gained from the use of UAS in coastal research. These operations could save time and money when compared with field surveys of elevation and vegetation. When in the field, there are fewer personnel requirements. UAS can overcome site accessibility issues, such as low water, offsetting the need for airboat access or the potential to trample part of a restoration site. UAS can deliver more frequent monitoring events and develop higher resolution structural models, surface elevation models, and multispectral orthomosaics of entire project sites. Conventional field methods collect point data along transects or coverage data using square meter plots. The UAS methods presented here develop continuous 2D surface models and classified datasets based on centimeter-level measurements over several square kilometers. In the case of the CRMS monitoring framework or restoration site monitoring, these datasets can capture previously unknown variability in the landscape by scaling from the plot to the landscape.

Finally, the ability to generate high-resolution maps of the land–water interface and quantify land loss, habitat fragmentation, biomass production, and carbon sequestration are particularly exciting. These map products would facilitate and improve estimation of valued ecosystem services, particularly at the project and landscape scale. The breadth of such assessments could not, at present, be coastwide or even regional. However, the potential is there to develop the fundamental methods and to slowly start increasing the extent of these endeavors, especially as technology advances in both long-distance UAS operations and big data analytics.

Future Research

A fair amount of research has recently been done using object-based image analysis on UAS imagery in coastal settings including herbaceous marshes (Meng et al. 2017), floating marshes (Pande-Chhetri et al. 2017), upland forests (Lechner et al. 2012), and mangroves (Cao et al. 2018). Recent developments in supervised classification using random tree analysis (Belluco et al. 2006; Michez et al. 2016), support vector machine learning, and artificial neural network techniques, also known as deep learning (Pande-Chhetri et al. 2017), have improved results. However, further research is needed to refine the object-based approach to UAS image classification. Radiometric corrections and standards will need to be set for larger regional analyses. The brightness and radiometry of UAS imagery are highly variable because of changing sun angles and weather patterns, and the use of commercial-grade sensors. This variability in the raw imagery will need to be addressed with consistent calibration practices if standardized approaches at larger regional scales are desired. Finally, standardized accuracy assessments of hyperspatial datasets collected with UAS are needed. Specifically, a statistical analysis of independent checkpoints is necessary to validate the absolute horizontal and vertical accuracy of the final products. The American Society for Photogrammetry and Remote Sensing recommends 20 such independent checkpoints (ASPRS 2015). As a rule of practice, the final accuracy statements should be no less than four times the accuracy of the equipment used to determine the location of the ground control and checkpoints. This ensures confidence in the estimates and accounts for errors in both the positioning system (i.e., GPS or leveling) and the photogrammetric process (i.e., Structure-from-Motion and bundle block adjustments) (Abdullah et al. 2015). Therefore, the need for multiple, fixed aerial targets surveyed with high-accuracy equipment remains a necessity for high-accuracy model development that meets current mapping standards. These standards will ensure that UAS products are comparable with previous conventional datasets and will support temporal analyses.

Another area of important and ongoing research is the estimation of plant biomass and carbon sequestration rates based on UAS imagery and subsequent datasets (Doughty and Cavanaugh 2019). If one can correctly classify the dominant plant species and plant height of an object, then standard coefficients could be used to calculate the biomass, productivity, and carbon sequestration. These coefficients would need to be based on experimental and observational datasets and dependent on the local conditions of the site in question. By knowing details about vegetative structure, coupled with hydrologic measures, estimates of sediment retention and storm surge attenuation could be made. The ability to scale field-based measurements to regional models remains a worthy goal and could lead to improved quantitative estimates of ecosystem services.

Acknowledgments The authors wish to thank Tom Cousté, Alvinette Teal, Shayne Teal, and Ben Landry with JESCO, Inc. for field support and for providing the UAS for data collection. Leigh Anne Sharpe with Louisiana Coastal Protection and Restoration Authority and Sarai Piazza and Brady Couvillion with the US Geological Survey supported the data analysis and collaboration on CRMS site 0392. Comments from Monique LaFrance Bartley and two anonymous reviewers greatly improved the quality of this manuscript. The work was funded in part by the University of Louisiana at Lafayette Institute for Coastal and Water Research.

References

Abdullah, Q., D. Maune, D. Smith, and H.K. Heidemann. 2015. New standard for new era: overview of the 2015 ASPRS positional accuracy standards for digital geospatial data. *Photogrammetric Engineering & Remote Sensing* 81 (3): 173–176.

Acosta, A., M.L. Carranza, and C.F. Izzi. 2005. Combining land cover mapping of coastal dunes with vegetation analysis. *Applied Vegetation Science* 8 (2): 133–138.

Ahmed, O.S., A. Shemrock, D. Chabot, C. Dillon, G. Williams, R. Wasson, and S.E. Franklin. 2017. Hierarchical land cover and vegetation classification using multispectral data acquired from an unmanned aerial vehicle. *International Journal of Remote Sensing* 38: 8–10.

American Society for Photogrammetry and Remote Sensing (ASPRS). 2015. ASPRS positional accuracy standards for digital geospatial data. *Photogrammetric Engineering & Remote Sensing* 81 (3): A1–A26.

Belluco, E., M. Camuffo, S. Ferrari, L. Modenese, S. Silvestri, A. Marani, and M. Marani. 2006. Mapping salt-marsh vegetation by multispectral and hyperspectral remote sensing. *Remote Sensing of Environment* 105 (1): 54–67.

Blaschke, T. 2010. Object based image analysis for remote sensing. *ISPRS Journal of Photogrammetry and Remote Sensing* 65 (1): 2–16.

Brooks, R.P., G.P. Patil, S. Fei, A.I. Gitelman, W.L. Myers, and E.D. Reavie. 2007. Next generation of ecological indicators of wetland condition. *EcoHealth* 4 (2): 176–178.

Broussard III, Whitney P, G.M. Suir, and J.M. Visser. 2018. Unmanned Aircraft Systems (UAS) and satellite imagery collections in a coastal intermediate marsh to determine the land–water interface, vegetation types, and Normalized Difference Vegetation Index (NDVI) values. US Army Corps of Engineers Wetlands Regulatory Assistance Program Report ERDC/TN-18-1 September 2018. pp. 1–17. doi: https://doi.org/10.21079/11681/29517.

Cao, J., W. Leng, K. Liu, L. Liu, Z. He, and Y. Zhu. 2018. Object-based mangrove species classification using unmanned aerial vehicle hyperspectral images and digital surface models. *Remote Sensing* 10 (2): 89.

Chamberlain, S.J., and H.M. Ingram. 2012. Developing coefficients of conservatism to advance floristic quality assessment in the mid-Atlantic region. *Journal of the Torrey Botanical Society* 139 (4): 416–427.

Chatagnier, J., 2012. The biomechanics of salt marsh vegetation applied to wave and surge attenuation. Louisiana State University, master thesis 1351. https://digitalcommons.lsu.edu/gradschooltheses/1351. Accessed 30 Dec 2019.

Chong, A.K. 2007. HD aerial video for coastal zone ecological mapping. In The 19th Annual Colloquium of the Spatial Information Research Centre.

Church, J.A., and N.J. White. 2006. A 20th century acceleration in global sea-level rise. *Geophysical Research Letters* 33: 94–97.

Chust, G., I. Galparsoro, Á. Borja, J. Franco, and A. Uriarte. 2008. Coastal and estuarine habitat mapping, using LIDAR height and intensity and multi-spectral imagery. *Estuarine, Coastal and Shelf Science* 78 (4): 633–643.

Coastal Protection and Restoration Authority (CPRA) of Louisiana. 2012. *Louisiana's comprehensive master plan for a sustainable coast*. Baton Rouge: Coastal Protection and Restoration Authority of Louisiana.

Coastal Protection and Restoration Authority (CPRA) of Louisiana. 2016. Coastwide Reference Monitoring System—Wetlands Monitoring Data. Retrieved from Coastal Information Management System (CIMS) database. http://cims.coastal.louisiana.gov. Accessed 12 December 2016.

Costanza, R., R. d'Arge, R. de Groot, S. Farberk, M. Grasso, B. Hannon, K. Limburg, S. Naeem, R.V. O'Neill, J. Paruelo, R.G. Raskin, P. Sutton, and M. van den Belt. 1997. The value of the world's ecosystem services and natural capital. *Nature* 387 (6630): 253–260.

Couvillion, B.R., H. Beck, D. Schoolmaster, and M. Fischer. 2017. Land Area Change in Coastal Louisiana (1932 to 2016) Scientific Investigations Map 3381. U.S. Geological Survey Scientific Investigations Map 3381, 16 p. pamphlet. doi: https://doi.org/10.3133/sim3381.

Cretini, K.F., J.M. Visser, K.W. Krauss, and G.D. Steyer. 2012. Development and use of a floristic quality index for coastal Louisiana marshes. *Environmental Monitoring and Assessment* 184 (4): 2389–2403.

Coastal Wetlands Planning Protection and Restoration Act (CWPPRA). (2008). Louisiana Aerial Photography: 2008 DOQQs.

DeLuca, W.V., C.E. Studds, R.S. King, and P.P. Marra. 2008. Coastal urbanization and the integrity of estuarine waterbird communities: threshold responses and the importance of scale. *Biological Conservation* 141 (11): 2669–2678.

Doughty, C., and K. Cavanaugh. 2019. Mapping coastal wetland biomass from high resolution unmanned aerial vehicle (UAV) imagery. *Remote Sensing* 11 (5): 540.

Eisenbeiss H 2004. A mini unmanned aerial vehicle (UAV): system overview and image acquisition. In: International Workshop on Processing and Visualizing Using High-Resolution Imagery.

Enwright, N.M., W.R. Jones, A.L. Garber, and M.J. Keller. 2014. Analysis of the impact of spatial resolution on land/water classifications using high-resolution aerial imagery. *International Journal of Remote Sensing* 35 (13): 5280–5288.

Giannini, M.B., and C. Parente. 2015. An object based approach for coastline extraction from Quickbird multispectral images. *International Journal of Engineering and Technology* 6 (6): 2698–2704.

Gilmore, M.S., E.H. Wilson, N. Barrett, D.L. Civco, S. Prisloe, J.D. Hurd, and C. Chadwick. 2008. Integrating multi-temporal spectral and structural information to map wetland vegetation in a lower Connecticut River tidal marsh. *Remote Sensing of Environment* 112 (11): 4048–4060.

Golley, Frank B. 1987. Deep ecology from the perspective of environmental science. *Environmental Ethics* 9 (1): 45–55.

González, J.L., and T.E. Tornqvist. 2006. Coastal Louisiana in crisis: subsidence or sea level rise? *Eos, Transactions of the American Geophysical Union* 87 (45): 493–508.

Gosselink, J.B. 1984. *The ecology of delta marshes of coastal Louisiana: a community profile. FWS/OBS-84/09*. Washington: U.S. Fish and Wildlife Service, Biological Services.

Hestir, E.L., S. Khanna, M.E. Andrew, M.J. Santos, J.H. Viers, J.A. Greenberg, S.S. Rajapakse, and S.L. Ustin. 2008. Identification of invasive vegetation using hyperspectral remote sensing in the California Delta ecosystem. *Remote Sensing of Environment* 112 (11): 4034–4047.

Husson, E., F. Ecke, and H. Reese. 2016. Comparison of manual mapping and automated object-based image analysis of non-submerged aquatic vegetation from very-high-resolution UAS images. *Remote Sensing* 8: 1–18.

Kent, M., and P. Coker. 1994. *Vegetation description and analysis: a practical approach*. West Sussex: J. Wiley and Sons.

Klemas, V. 2013. Airborne remote sensing of coastal features and processes: an overview. *Journal of Coastal Research* 29 (2): 239–255.

Klemas, V. 2015. Coastal and environmental remote sensing from unmanned aerial vehicles: an overview. *Journal of Coastal Research* 315 (5): 1260–1267.

Laliberte, A.S., and A. Rango. 2009. Texture and scale in object-based analysis of subdecimeter resolution unmanned aerial vehicle (UAV) imagery. *IEEE Transactions on Geoscience and Remote Sensing* 47 (3): 761–770.

Lechner, A.M., A. Fletcher, K. Johansen, and P. Erskine. 2012. Characterising upland swamps using object-based classification methods and hyper-spatial resolution imagery derived from an unmanned aerial vehicle. *ISPRS Annals of Photogrammetry, Remote Sensing and Spatial Information Sciences* I-4: 101–106.

Lejot, J., C. Delacourt, H. Piégay, T. Fournier, M. Trémélo, and P. Allemand. 2007. Very high spatial resolution imagery for channel bathymetry and topography from an unmanned mapping controlled platform. *Earth Surface Processes and Landforms* 32 (11): 1705–1725.

Mancini, F., M. Dubbini, M. Gattelli, F. Stecchi, S. Fabbri, and G. Gabbianelli. 2013. Using unmanned aerial vehicles (UAV) for high-resolution reconstruction of topography: the structure from motion approach on coastal environments. *Remote Sensing* 5 (12): 6880–6898.

Marceau, D., and G.J. Hay. 1999. Contributions of remote sensing to the scale issue. *Canadian Journal of Remote Sensing* 25 (4): 357–366.

Marcaccio, J.V., C.E. Markle, and P. Chow-Fraser. 2015. Unmanned aerial vehicles produce high-resolution, seasonally-relevant imagery for classifying wetland vegetation. *The International Archives of the Photogrammetry, Remote Sensing and Spatial Information Sciences* 40: 249–256.

Meckel, T.A., U.S. ten Brink, and S.J. Williams. 2006. Current subsidence rates due to compaction of Holocene sediments in southern Louisiana. *Geophysical Research Letters* 33: 1–5.

Michez, A., H. Piégay, L. Jonathan, H. Claessens, and P. Lejeune. 2016. Mapping of riparian invasive species with supervised classification of unmanned aerial system (UAS) imagery. *International Journal of Applied Earth Observation and Geoinformation* 44: 88–94.

Meng, X., N. Shang, X. Zhang, C. Li, K. Zhao, X. Qiu, and E. Weeks. 2017. Photogrammetric UAV mapping of terrain under dense coastal vegetation: an object-oriented classification ensemble algorithm for classification and terrain correction. *Remote Sensing* 9: 1–23.

Mitchell, M.K., B.M. Ballard, J.M. Visser, M.G. Brasher, and E.J. Redeker. 2014. Delineation of coastal marsh types along the Central Texas coast. *Wetlands* 34 (4): 653–660.

Moreau, S., and T. Le Toan. 2003. Biomass quantification of Andean wetland forages using ERS satellite SAR data for optimizing livestock management. *Remote Sensing of Environment* 84 (4): 477–492.

Morris, J.T., P.V. Sundareshwar, C.T. Nietch, B. KJerfve, and D.R. Cahoon. 2002. Responses of coastal wetlands to rising sea level. *Ecology* 83 (10): 2869–2877.

Morris, J.T., D.C. Barber, J.C. Callaway, R. Chambers, S.C. Hagen, C.S. Hopkinson, B.J. Johnson, P. Megonigal, S.C. Neubauer, T. Troxler, and C. Wigand. 2016. Contributions of organic and inorganic matter to sediment volume and accretion in tidal wetlands at steady state. *Earth Future* 4 (4): 110–121.

Nahlik, A.M., and M.S. Fennessy. 2016. Carbon storage in US wetlands. *Nature Communications* 7 (1): 13835.

Niethammer, U., M.R. James, S. Rothmund, J. Travelletti, and M. Joswig. 2012. UAV-based remote sensing of the Super-Sauze landslide: evaluation and results. *Engineering Geology* 128: 2–11.

O'Neil-Dunne, J., S. MacFaden, and A. Royar. 2014. A versatile, production-oriented approach to high-resolution tree-canopy mapping in urban and suburban landscapes using GEOBIA and data fusion. *Remote Sensing* 6 (12): 12837–12865.

Pande-Chhetri, R., A. Abd-Elrahman, T. Liu, J. Morton, and V.L. Wilhelm. 2017. Object-based classification of wetland vegetation using very high-resolution unmanned air system imagery. *European Journal of Remote Sensing* 50 (1): 564–576.

Pereira, E., R. Beneatel, J. Correia, L. Felix, G. Goncalves, J. Morgado, and J. Sousa. 2009. Unmanned air vehicles for coastal and environmental research. *Journal of Coastal Research* 56: 1557–1561.

Phinn, S.R., D.A. Stow, and J.B. Zedler. 1996. Monitoring wetland habitat restoration in southern California using airborne multi spectral video data. *Restoration Ecology* 4 (4): 412–422.

Przybilla, H., and W. Wester-Ebbinghaus. 1979. Bildflug mit ferngelenktem Kleinflugzeug. *Bildmessung und Luftbildwessen* 47: 137–142.

Rebelo, L.M., C.M. Finlayson, and N. Nagabhatla. 2009. Remote sensing and GIS for wetland inventory, mapping and change analysis. *Journal of Environmental Management* 90 (7): 2144–2153.

Sankey, T., J. Donager, J. McVay, and J.B. Sankey. 2017. UAV lidar and hyperspectral fusion for forest monitoring in the southwestern USA. *Remote Sensing of Environment* 195: 30–43.

Sasser, C.E., J.M. Visser, E. Mouton, J. Linscombe, and S.B. Hartley. 2014. Vegetation types in coastal Louisiana in 2013. U.S. Geological Survey Scientific Investigations Map 3290, 1 Sheet, Scale 1:550,000, 3290. doi: https://doi.org/10.3133/sim3290

Schoolmaster, D.R., C.L. Stagg, L.A. Sharp, T.E. McGinnis, B. Wood, and S.C. Piazza. 2018. Vegetation cover, tidal amplitude and land area predict short-term marsh vulnerability in coastal Louisiana. *Ecosystems* 21 (7): 1335–1347.

Steyer, G.D. 2010. Coastwide Reference Monitoring System (CRMS): U.S. Geological Survey Fact Sheet 2010–3018, 2 p. https://pubs.usgs.gov/fs/2010/3018/. Accessed 20 Dec 2017.

Steyer, G.D., B.R. Couvillion, and J.A. Barras. 2013. Monitoring vegetation response to episodic disturbance events by using multitemporal vegetation indices. *Journal of Coastal Research* 63: 118–130.

Suir, G.M., D.E. Evers, G.D. Steyer, and C.E. Sasser. 2013. Development of a reproducible method for determining quantity of water and its configuration in the marsh landscape. *Journal of Coastal Research* 63: 110–117.

Trimble Inc. 2016a. Inpho UASMaster v7.1. [software] Retrieved from: https://geospatial.trimble.com/products-and-solutions/trimble-inpho-uasmaster. Accessed 2 Jun 2016.

Trimble Inc. 2016b. eCognition developer v9.1. [software] Retrieved from: http://www.ecognition.com. Accessed 2 Jun 2016.

Valdes, K., E.A. Hunter, and N.P. Nibbelink. 2016. Salt marsh elevation is a strong determinant of nest-site selection by clapper rails in Georgia, USA. *Journal of Field Ornithology* 87 (1): 65–73.

Visser, J.M., C.E. Sasser, R.H. Chabreck, and R.G. Linscombe. 1998. Marsh vegetation types of the Mississippi River deltaic plain. *Estuaries* 21 (4): 818–828.

Wang, F., X. Lu, C.J. Sanders, and J. Tang. 2019. Tidal wetland resilience to sea level rise increases their carbon sequestration capacity in United States. *Nature Communications*.019-13294-z.

Westoby, M.J., J. Brasington, N.F. Glasser, M.J. Hambrey, and J.M. Reynolds. 2012. 'Structure-from-motion' photogrammetry: a low-cost, effective tool for geoscience applications. *Geomorphology* 179: 300–314.

Woodrey, M.S., S.A. Rush, J.A. Cherry, B.L. Nuse, R.J. Cooper, and A.J.J. Lehmicke. 2012. Understanding the potential impacts of global climate change on marsh birds in the Gulf of Mexico region. *Wetlands* 32 (1): 35–49.

Yang, B., and C. Chen. 2015. Automatic registration of UAV-borne sequent images and LiDAR data. *ISPRS Journal of Photogrammetry and Remote Sensing* 101: 262–274.

Yang, J., and F.J. Artigas. 2010. Mapping salt marsh vegetation by integrating hyperspectral and LiDAR remote sensing. In *Remote sensing of coastal environments*, ed. Y. Wang, 173–190. Boca Raton: CRC Press.